Thermoresponsive Behavior of Micellar Aggregates from end-functionalized PnBA-b-PNIPAM-COOH Block Copolymer and their Complexes with Lysozyme

Aristeidis Papagiannopoulos[1,*], Anastasia Meristoudi[1], Stergios Pispas[1,*] and Uwe Keiderling[2]

[1]Theoretical and Physical Chemistry Institute, National Hellenic Research Foundation, 11635 Athens, Greece

[2]Helmholtz Zentrum Berlin, D-14109 Berlin, Germany

* pispas@eie.gr

* apapagiannopoulos@eie.gr

Abstract

The temperature response of micellar aggregates of poly(n-butyl acrylate)-b-poly(N-isopropylacrylamide)-carboxylic acid (PnBA-b-PNIPAM-COOH) end-functionalized diblock copolymers in aqueous solutions is investigated by small angle neutron scattering and light scattering techniques. The particular micellar aggregates present –COOH groups at their surface due to the molecular architecture of the block copolymer chains. Above the critical solution temperature micellar aggregation depends on the initial solution concentration, while at the highest polymer contents intermicellar correlations are observed as a hard-sphere interaction intensity peak. Addition of lysozyme induces this morphological transition even at low concentrations. The scattering profiles are consistent with lysozyme accumulating in the vicinity of the micellar cores a finding that is supported by measurements in lysozyme contrast matched solvent. Upon temperature increase negatively charged units are exposed to the surface of the aggregates during the thermal transition which

is a stabilizing force against the phase separating coil-to-globule transition of poly(N-isopropylacrylamide) (PNIPAM).

Introduction

Protein interactions with macromolecular nanostructures have been investigated intensely during the last two decades because of the high potential for application in protein separation, drug delivery, food science and tissue engineering[1]. Complexation of proteins with polyelectrolytes is dictated by complex physical phenomena that involve Coulomb interactions specific to protein charge anisotropy and local pH values.[1,2] Small angle scattering methods and analysis advancements has pushed the field forward by characterizing in detail not only the morphology of protein binding nanoparticles e.g. spherical polyelectrolyte brushes, but also the location of adsorbed protein globules[3]. In other works contrast variation and selective labeling in small angle neutron scattering (SANS) has been exploited to define the conformational alterations of both the macromolecular and protein component during interaction[4]. Electrostatic interactions, entropic counterion release forces[5] and hydrophobic interactions take part in protein polyelectrolyte binding[6].

At the same time PNIPAM-containing polymers are under extensive study[7, 8] due to the well documented volume phase transition of PNIPAM in water[9] at physiological relevant temperature, which makes it a highly desirable component for stimuli responsive nanocarriers,[10] in tissue engineering and biosensors[11] and in the general field of smart materials[12]. In block copolymers thermoresponsive PNIPAM blocks can induce transitions from hierarchical aggregates at room temperature to well defined structures above the lower critical solution temperature (LCST)[13] when the other block is hydrophilic. When the other block is hydrophobic micellar structures are self-

assembled to higher aggregates with well documented kinetics[14] and internal arrangement[15, 16]. Recently we have demonstrated that complexation of lysozyme with aggregates of a doubly responsive poly(ethylene oxide)-b-poly(N-isopropylacrylamide)-b-poly(acrylic acid) (PEO-b-PNIPAM-b-PAA) triblock terpolymer[17] enhances the internal hydrophobic associations and renders the thermoresponsive internal collapse totally irreversible.

In this article we investigate the temperature-responsive morphology of PnBA-b-PNIPAM-COOH (poly(n-butyl acrylate)-b-poly(N-isopropylacrylamide)-carboxylic acid) self-assembled hierarchical aggregates and the effects of interaction with lysozyme. We present a detailed small angle scattering analysis of the sensitivity of temperature response on polymer concentration and demonstrate how complexation of lysozyme enhances the transition to aggregated interacting hard-core micelles at low concentrations. This study aims to extend the detailed morphological analysis of nanoparticle protein complexes and thermoresponsive self-assembled structures to protein loaded thermoresponsive nanostructures.

Experimental

Synthesis of PnBA-b-PNIPAM-COOH end-functionalized amphiphilic block copolymer

n-butylacrylate (nBA, Aldrich) monomer was distilled in a vacuum line prior to use. *N*-isopropylacrylamide (NIPAM, Aldrich) was recrystallized twice from benzene/n-hexane (1:4). 4,4′-azobis(isobutyronitrile) (AIBN), from Fluka, was recrystallized from ethanol and subsequently used as a solution in dioxane. 1,4-dioxane (Aldrich) was dried over molecular sieves. S-1-Dodecyl-S$^{'}$-(α,α$^{'}$-dimethyl-α$^{''}$-acetic acid)trithiocarbonate (DTTC) was the chain transfer agent (CTA), obtained from Aldrich and utilized as received.

PnBA-b-PNIPAM-COOH amphiphilic block copolymer was synthesized by Reversible addition−fragmentation chain-transfer polymerization (RAFT), as described earlier[18], with the difference being the order of monomer polymerization sequence. In this work NIPAM was polymerized first. The resulting macromolecular PNIPAM CTA was used for the polymerization of nBA in the presence of additional AIBN as radical initiator. The particular reaction scheme places a –COOH group, resulting from CTA fragmentation, at the free end of the PNIPAM hydrophilic/thermoresponsive block (scheme 1). Therefore, subsequent dissolution of the PnBA-b-PNIPAM-COOH block copolymer in water gives micelles with –COOH residing at their surface. Characterization of the block copolymer by SEC, in THF/3%v/v Et_3N, and ^{1}H-NMR, in $CDCl_3$, gave the following molecular characteristics, M_w=10,300, M_w/M_n= 1.21, 30%wt PnBA. Consequently the degrees of polymerization are 24 for PnBA and 65 for PNIPAM.

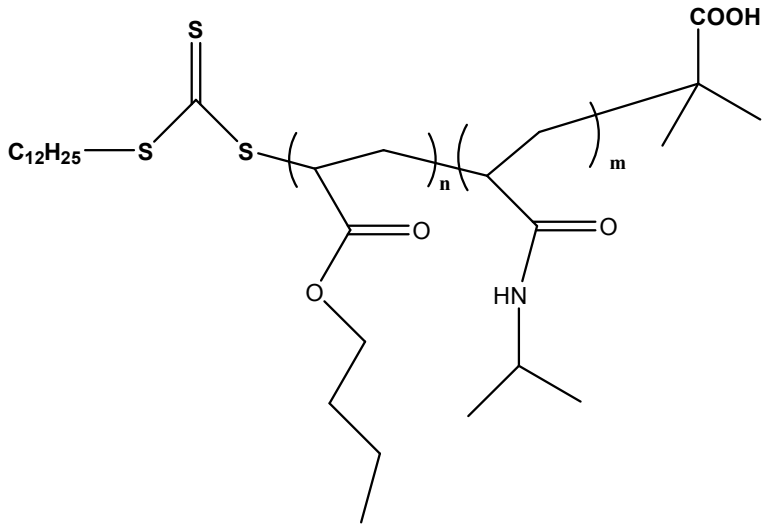

Scheme 1: Molecular structure of the PnBA-b-PNIPAM-COOH end-fuctionalized amphiphilic block copolymer.

Sample Preparation

PnBA-b-PNIPAM-COOH powder was dissolved in water (H_2O for light scattering and H_2O/D_2O mixtures for small angle neutron scattering) in order to make parent solutions which were then diluted by the same solvent to the target concentrations. The salt content was set to 0.01M by NaCl and the pH of the final solutions was tuned to 7 by adding small amounts of HCl or NaOH (DCl or NaOD for neutron experiments). Lysozyme stock solutions (lysozyme HEWL was purchased from Fluka and used without further treatment) were prepared by dissolving protein in the appropriate H_2O/D_2O mixture in 0.01M NaCl at pH 7.

Small Angle Neutron Scattering

Experiments were performed on the Small Angle Neutron Scattering (SANS) instrument V4 (BERII Reactor at HZB). Scattering vectors (q) from 0.002 to 0.5 $Å^{-1}$ was covered by three separate detection/wavelength configurations i.e. 16m/1.174nm, 4m/0.506nm and 1.35m/0.506nm. For the low-q regime of weak forward-scattering samples (H_2O/D_2O mixed solvents) 12m/0.506nm configuration was used. In SANS the scattered intensity $I(q)$ is collected by a 2-D detector in the form of azimuthally isotropic patterns (normal for dilute solutions) which is afterwards azimuthally integrated leading to the 1-D. The 2-D raw data are corrected for the scattering from the empty cell and the solvent and the electronic and background noise. BerSANS software developed by U. Keiderling[19] was used for data reduction. Resolution in q is taken into account[20] by equation 1 where the standard deviation in wave vector of V4 ($\Delta\lambda/\lambda = 0.10$) is the dominant contribution i.e. $\Delta q(q)/q = \Delta\lambda/\lambda$. The convoluted curves $I^{conv}(q)$ are the ones fitted against the experimentally obtained data $I(q)$.

$$I^{conv}(q) = \frac{1}{\sqrt{2\pi}\Delta q(q)} \cdot \int_{-\infty}^{+\infty} dq' \cdot exp\left(-\left(\frac{q'-q}{\sqrt{2}\Delta q(q)}\right)^2\right) \cdot I^{th}(q') \qquad (1)$$

The data was fitted by minimizing the sum of the weighted square differences $\chi^2 = \sum_{i=1}^{N} \left(\frac{I^{conv}(q_i) - I^{exp}(q_i)}{\delta I^{exp}(q_i)} \right)^2$ between the N theoretical and experimental data points. The nonlinear least square optimization was performed by the Monte Carlo algorithm in a simulated annealing process[21] by custom made code in MATLAB.

The temperature of the samples was controlled with an accuracy of 0.1ºC and the samples were left to equilibrate for longer than 30 minutes at the set temperature.

Static, Dynamic and Electrophoretic Light Scattering

An ALV/CGS-3 compact goniometer system (ALVGmbH, Germany), equipped with an ALV-5000/EPP multi tau digital correlator and a He-Ne laser operating at the wavelength of 632.8 nm was used. In Static Light Scattering (SLS) the Rayleigh ratio $R(q)$ was calculated with respect to a toluene standard at a series of angles in the range 30-120°. The scattering wave vector is given by $q = \frac{4\pi n_0}{\lambda} sin\frac{\theta}{2}$ where n_0 is the solvent's refractive index.

SLS data were treated[22] by equation 2.

$$\frac{Kc}{R(q,c)} = \frac{1}{M_w P(q)} \qquad (2)$$

where M_w is the weight-averaged molar mass and c is the particle concentration in solution. The single particle's form factor was treated by the Guinier approximation $P(q) = e^{-\frac{1}{3}q^2 R_{g,SLS}^2}$, where$R_{g,SLS}^2$ the radius of gyration obtained by SLS. K is the contrast factor for LS given by $K = \frac{4\pi^2 n_0^2}{N_A \lambda^4} (\partial n/\partial c)^2$, where $\partial n/\partial c$ is the refractive index increment of the scattering particles in the solvent.

In Dynamic Light Scattering (DLS) the intensity auto-correlation functions $g^{(2)}(t)$ are collected [23] at certain scattering angle and are analysed by the CONTIN algorithm. The characteristic relaxation rate $\Gamma(q)$ is taken from the position of the maximum

($\tau(q)$) of the distribution function of relaxation times ($\Gamma(q) = \frac{1}{\tau(q)}$). In the case of diffusive modes there is a linear relation between $\Gamma(q)$ and q^2 i.e. $\Gamma(q) = D \cdot q^2$ and hence the diffusion coefficient D is obtained. The hydrodynamic radius, R_h, is extracted from the Stokes-Einstein equation (equation 3).

$$R_h = \frac{k_B T}{6\pi\eta D} \qquad (3)$$

where η is the viscosity of the solvent, k_B is the Boltzmann constant and T is the absolute temperature. All the LS experiments were performed at controlled temperature which was set by a PolyScience temperature controller and it was proved that 15min wait was enough for the samples to equilibrate.

Zeta potential measurements were performed on a Zetasizer Nano-ZS by Malvern Instruments Ltd.. The calculation was made by Henry equation in the Smoluchowski approximation. The ζ values reported are averages of 10-20 measurements taken at 173° angle.

Results & discussion

Self-assembly of PnBA-b-PNIPAM-COOH

At room temperature PNIPAM is in good solvent conditions and hence COOH-terminated PNIPAM chains are expected to be well dissolved in water. The hydrophobicity of PnBA block (not expected to depend strongly on temperature) will force PnBA-b-PNIPAM-COOH chains to form amphiphilic core-shell micelles. Monitoring the scattered light intensity at a fixed angle for different temperatures is a sensitive probe of transitions in solutions[24]. PNIPAM's coil-to globule transition in water causes an abrupt increase of the scattered intensity around 40 °C (figure 1). Apparently, this illustrates the molecular weight increase of the scattering objects or in other words association between the micelles that already exist at room temperature (see further discussion for confirmation of micellar morphology). The increased

hydrophilicity of the system because of the presence of fully charged end carboxylic units at pH 7 is a possible cause for the LCST appearing at temperatures higher than 32 ºC [24]. Nevertheless a more complicated mechanism may be involved since the transition observed by our scattering methods is dominated by morphological changes at higher aggregation states.

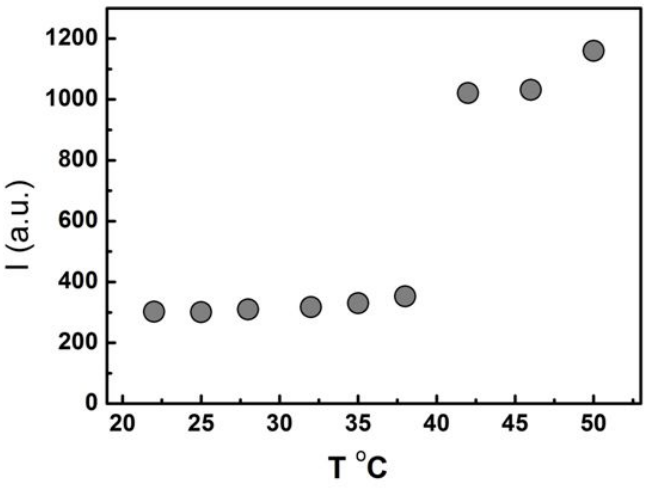

Figure 1: Static light scattering intensity ($\theta = 90°$) from PnBA-b-PNIPAM-COOH at $c = 0.01\ mg/ml$ as a function of temperature.

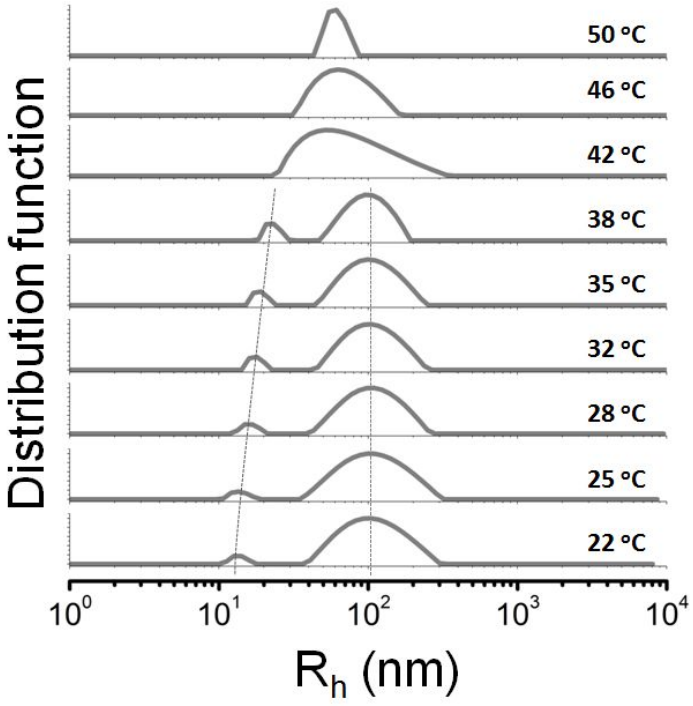

Figure 2: Size distribution function of PnBA-b-PNIPAM-COOH at $c = 0.01\ mg/ml$ obtained by CONTIN analysis of the DLS autocorrelation functions ($\theta = 90°$) at several solution temperatures. Dotted lines are guides to the eye.

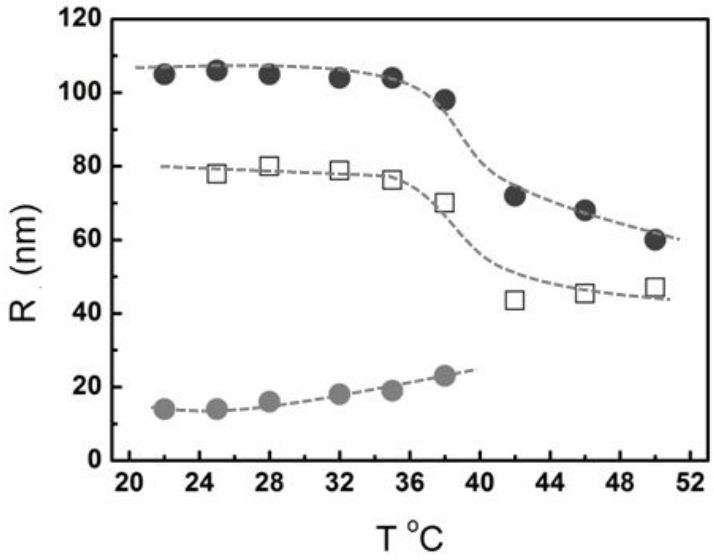

Figure 3: Hydrodynamic radii of micelles (●) and aggregates (●) obtained by DLS and radius of gyration (□) obtained by SLS in PnBA-b-PNIPAM-COOH solutions at $c = 0.01\ mg/ml$ at several solution temperatures. Dashed lines are guides to the eye.

In figure 2 the distributions of hydrodynamic radii obtained by CONTIN analysis reveal two sizes at room temperature. There is a small-size population (~20nm) that shows a weak increase as temperature increases. This size is more probable to correspond to aggregated PnBA-b-PNIPAM-COOH chains and not single isolated ones because in that case[13] their hydrodynamic radius would not be higher than 4-5 nm. For doubly hydrophilic PEO-b-PNIPAM isolated chains of roughly 10 times higher degree of polymerization[13] we have observed $R_g \approx 4.6\ nm$. The size of a fully extended PnBA-b-PNIPAM-COOH chain would be about 20 nm but this would not be expected for an isolated chain in a good solvent. Even in that case R_h would not

exceed 10 nm. The dominant population (~110nm) is fairly constant in size up to 38 °C. This population corresponds to aggregates in a higher hierarchical level i.e. aggregates of micelles as will be illustrated in the following SANS discussion. Above 40 °C there is only one single peak that becomes significantly narrower at high temperatures. This transition that was also seen in the scattered light intensity signifies that above the LCST of PnBA-b-PNIPAM-COOH large aggregates dominate the population in solution. Additionally their size and morphology becomes better defined as indicated by the narrow peak at 50 °C. The slight increase in micellar hydrodynamic radius with temperature indicates an enhancement of their aggregation number (figure 3). It is known that weak hydrophobic interactions between PNIPAM chains may begin below PNIPAM's LCST [9, 17, 24, 25]. Aggregates R_h is constant below the transition temperature (40 °C) and drops abruptly afterwards. This may reflect the shrinkage of PNIPAM chains and consequently the aggregates size. Apparent R_g follows the trend of R_h possibly because the scattering is dominated by the large size population. Their ratio is ~0.72 which is compatible with a spherical morphology with uniform mass distribution[17, 26]. As observed by ζ-potential measurements at high temperatures (see discussion on complexation) the COO^- units per aggregate seem higher in number and also exposed to the aggregate surface compared to the low temperature (-27mV at 43°C, -2.0mV at 25°C). This supports the hypothesis that the hydrophilic-hydrophobic transition of PNIPAM creates particles with a hard hydrophobic interior and soft hydrophilic charged surface.

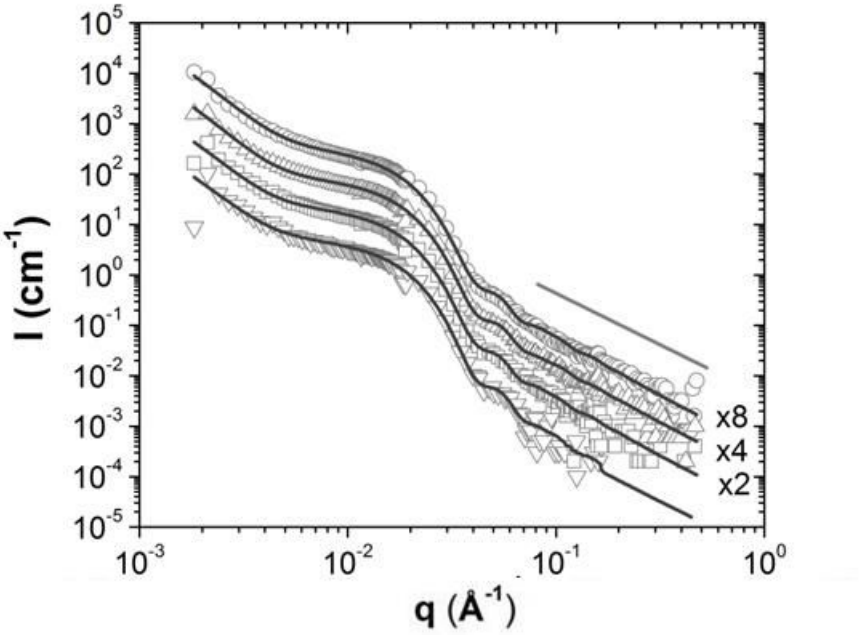

Figure 4: SANS scattered intensity from PnBA-b-PNIPAM-COOH at 25° C for 0.5 (▽), 1.0 (□), 2.0 (△) and 4.0 (○) mg/ml in D_2O. Lines are best fits with equation 4. Straight line is a power-law q^{-2}. Curves have been multiplied by indicated factors for clarity.

At room temperature the shape of the SANS curves showed no dependence on concentration (from 0.5 to 4 mg/ml) while their magnitude scaled linearly with concentration. The data was modeled by a combination of monodisperse spherical core-shell micelles and large aggregates (equation 4). The quality of the fits is presented in figures 4 and 6. The presence of aggregates is supported by the LS results and expressed in SANS by the upturn curves at $q < 4 \cdot 10^{-3}\text{Å}^{-1}$. The weak drop of intensity at $5 \cdot 10^{-3}\text{Å}^{-1} < q < 1 \cdot 10^{-2}\text{Å}^{-1}$ (Guinier regime of micelles), the following strong drop and the characteristic weak oscillation bump at $q = 5.5 \cdot 10^{-2}\text{Å}^{-1}$ are common for well-defined core-shell objects in solution[22, 27]. The high q regime scales roughly as q^{-2} and hence cannot be followed by the spherically

symmetric model which scales as q^{-4}. This regime is modeled by introducing the scattering from correlations within the corona of the micelles.[16]

$$I(q) = I_{agg}(q) + I_{mic}(q) + I_{int}(q) \qquad (4)$$

The term $I_{agg}(q)$ is the scattering from large aggregates which is written (equation 5) as the combination of a Guinier (dominant at large length scales) term bridged with a power-law dependence (dominant at small length scales) and provides the radius of gyration (R_g), fractal exponent (d_{agg}) and scattering strength (G_{agg}) of the objects.[22, 28]

Prefactors are related by $B_{agg} = \frac{G_{agg} \cdot d_{agg}}{R_g^{d_{agg}}} \cdot \left[\frac{6{d_{agg}}^2}{(2+d_{agg})(2+2d_{agg})}\right]^{d_{agg}/2} \Gamma\left(\frac{d_{agg}}{2}\right)$ and this is similar for equation 6.

$$I_{agg}(q) = G_{agg} \cdot exp\left(-\frac{q^2 R_g^2}{3}\right) + \frac{B_{agg}}{q^{d_{agg}}}\left[erf\left(-\frac{qR_g}{\sqrt{6}}\right)\right] \qquad (5)$$

The intramicellar blob scattering $I_{int}(q)$ is modeled by a scattering function same as in equation 5 although only the power-law term gives significant scattering compared to the other two terms I_{agg} and I_{mic} (see figure 6). Hence the characteristic length scale ξ_{int} and the prefactor g_{int} are not resolved by the fits.

$$I_{int}(q) = g_{int} \cdot exp\left(-\frac{q^2 \xi_{int}^2}{3}\right) + \frac{B_{int}}{q^{d_{int}}}\left[erf\left(-\frac{q\xi_{int}}{\sqrt{6}}\right)\right] \qquad (6)$$

The micellar term $I_{mic}(q)$ is modeled by the single-particle scattering from spherically symmetric objects (equation 7) that is defined by the particle number density N_{mic} and the neutron scattering contrast between the particle $\rho(r)$ and the solvent[29] ρ_{water}. The integration in equation 7 is performed numerically by the Filon rule[30] which is suitable for strongly oscillating functions.

$$I_{mic}(q) = N_{mic} \cdot \left\{4\pi \int_0^{\infty} (\rho(r) - \rho_{water})\, r^2 \frac{sinqr}{qr} dr\right\}^2 \qquad (7)$$

A core-shell profile where the core has uniform neutron contrast and the shell a varying one[16, 31] was used for the profile $\rho(r)$ as in equation 8. Particle neutron scattering length density is connected to the polymer volume fraction by $\rho_{core} = \varphi_{core} \cdot \rho_{av} + (1 - \varphi_{core}) \cdot \rho_{water}$ and $\rho_{sh}(r) = \varphi(r) \cdot \rho_{av} + \big(1 - \varphi(r)\big) \cdot \rho_{water}$. The volume fraction in the shell is assumed to be a decaying function of r i.e. $\varphi(r) = \varphi_0 \cdot \left(\frac{r}{R_c}\right)^{-\alpha}$.

$$\rho(r) = \begin{cases} \rho_{core}\ for\ 0 \le r < R_c \\ \rho_{sh}(r)\ for\ R_c \le r < R_m \end{cases} \qquad (8)$$

As can been seen from figure 6 the contribution of the three terms is clearly separated which makes the parameters of each term independently defined from the others. The micellar form factor contains N_{mic}, φ_{core}, R_c, φ_0, R_m and α. The last four parameters are fitted while N_{mic} is calculated by the resulting aggregation number and the nominal solution concentration. The need of this core-shell form factor is justified by the failure to fit with homogeneous spheres or homogeneous core-homogeneous

shell profile (even including polydispersity). The high-q term is needed as a spherical core-shell profile cannot follow this power-law trend as discussed above.

Our fits lead to significantly higher number of PnBA chains compared to PNIPAM chains per micelle if we suppose that the core consists only of hydrophobic PnBA segments, while the shell contains only PNIPAM chains. This obliges us to assume that both PnBA and PNIPAM segments are present in both the core and the shell. Bokias et al. have demonstrated that PNIPAM interacts with hydrophobically modified polymers at room temperature.[32] Hence this inherent hydrophobic content of PNIPAM below the LCST can in our case cause association with the hydrophobic units of PnBA providing them a stable environment even in the presence of water molecules. This way random interchain hydrophobic contacts between PnBA and PNIPAM are formed. A compact uniform concentration near the centre (dense core) and a diffuse corona is the resulting morphology as extracted by SANS. We should also mention that the interaction of PNIPAM with hydrophobically modified polymers[32] leads to an increase in LCST, a qualitatively similar result demonstrated by our SLS and DLS data (figures 1-3).

For our SANS model calculations we use a block-volume-weighted average neutron scattering length density contrast ρ_{av} for the macromolecular chains. The fitted profiles $\rho(r)$ are able then to provide the average numbers of chains within the core (N_{in}) and the shell (N_{out}) if the mass concentration of micelles is taken equal to the solution concentration. For all cases φ_{core}~80% is always higher than φ_0~60% which means that micelles are formed by a dense core and a highly hydrated shell.

The evolution of SANS data as temperature increases is shown in figure 5. The low q upturn is enhanced greatly at 50 °C in a manner that at this temperature a single power-law behaviour extends up to $2 \cdot 10^{-2}\text{Å}^{-1}$. At 40 °C (region of

thermoresponsive transition) the presence of aggregates is slightly enhanced for the two lowest concentrations as the curve shape is not greatly changed. At 40 °C SANS data of 2.0 mg/ml shows signs of enhanced low-q power-law behavior i.e. characteristic of the situation at 50 °C. PNIPAM containing amphiphilic copolymers[16] show great sensitivity in concentration near the transition temperature and in this work it is clear that the different number of same kind of micellar aggregates in solution at room temperature results to different self-assembly motifs at higher temperatures. The situation of the highest temperature (4.0 mg/ml) is most illustrative. The scattering profile qualitatively changes even from 40 °C. A single power-law shifted towards even smaller length scales dominates low q region, while at intermediate scattering vectors a characteristic correlation peak is observed. The small length scale intra-micellar correlation is the only q regime that remains intact by temperature at this concentration.

Table 1: SANS extracted parameters for PnBA-b-PNIPAM-COOH at the studied concentrations and temperatures. The estimated uncertainty is ~2% for the radii and up to 5% for the rest of the parameters.

Conc. $(\frac{mg}{ml})$/	**25 °C**				**40 °C**				**50 °C**			
Param.	0.5	1.0	2.0	4.0	0.5	1.0	2.0	4.0	0.5	1.0	2.0	4.0
$R_c(nm)$	6.1	6.2	6.0	6.2	6.4	6.4	6.4	6.3	6.5	6.4	6.4	6.4
$R_m(nm)$	16.6	16.8	16.6	16.7	18.4	18.4	18.4	17.8	18.33	18.2	18.0	16.3
$t_s(nm)$	10.5	10.5	10.6	10.5	12.0	12.0	12.0	11.4	11.80	11.8	11.7	9.90
N_{in}	49	56	49	51	72	73	54	5	43	31	31	3
N_{out}	233	251	241	224	348	364	263	14	191	135	134	7

N_{tot}	282	207	290	275	420	437	317	19	234	166	165	10
a	1.70	1.73	1.73	1.77	2.13	2.13	2.17	2.11	2.29	2.30	2.30	2.11
$I_0(cm^{-1})$	5.5	11.9	22.5	42.5	8.1	16.8	24.5	2.3	4.5	6.8	12.8	1.63
$G_{agg}(cm^{-1})$	850	1930	4710	10800	1860	2980	2550	24400	97100	102100	264300	9340
d_{agg}	3.80	3.88	3.93	3.84	3.99	3.86	1.81	3.95	3.08	2.91	2.95	4.01
$R_g(nm)$	168	161	161	165	180	161	167	164	378	333	359	160
d_{int}	2.00	2.03	2.03	2.04	2.10	2.08	1.96	2.08	2.60	2.40	2.60	1.98
φ_{hs}								0.26				0.25
D_{hs}								18.6				18.6

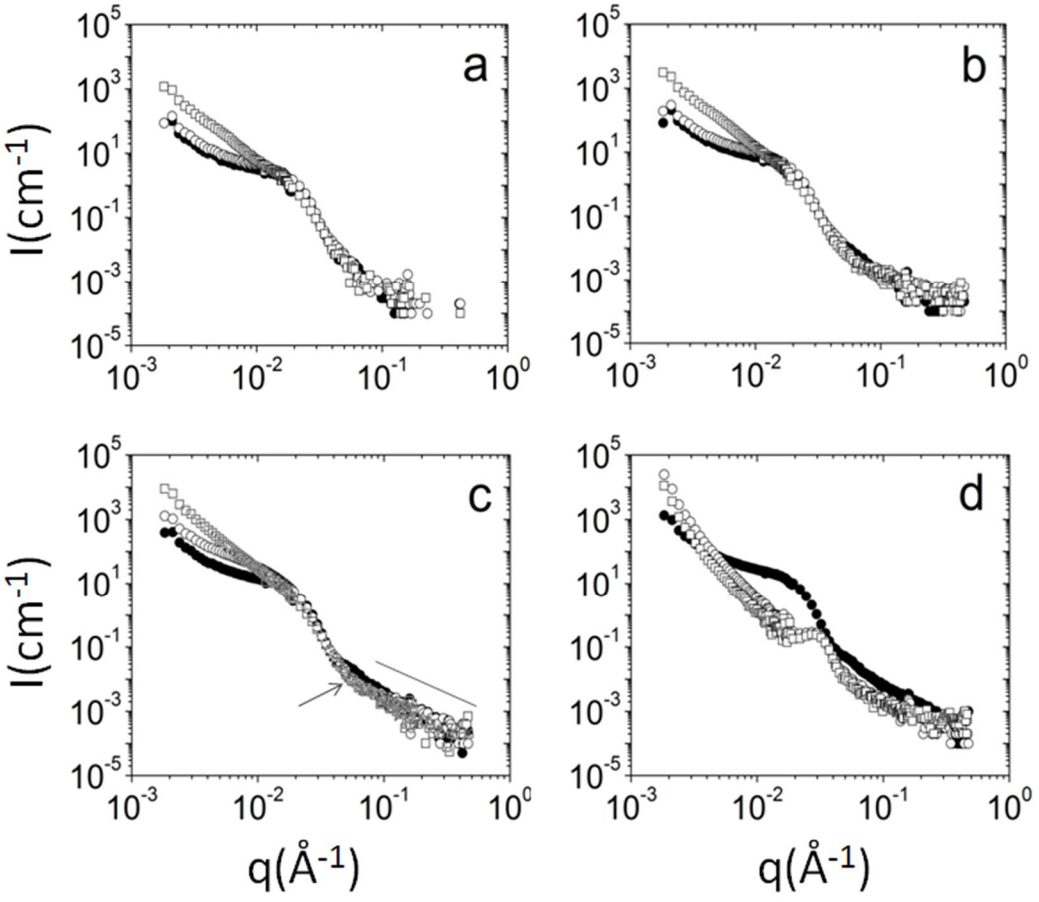

Figure 5: SANS data from PnBA-b-PNIPAM-COOH for different concentrations (a) 0.5, (b) 1.0, (c) 2.0 and (d) 4.0 mg/ml and different temperatures 25 (●), 40 (○) and 50 (□) °C. Straight line represents q^{-2} scaling.

Smearing of the characteristic oscillation (indicated by the arrow in figure 5c) signifies the change in internal morphology that occurs at higher temperatures and it is defined by the fitting parameters as both a slight increase of the core radius and an increase in the exponent a (table 1). At the same time the micellar radius and the shell thickness are found higher at 40 and 50 °C. These trends reflect an enhancement of the number of PnBA-b-PNIPAM-COOH chains both in the core (N_{in}) and in the shell (N_{out}) that is shown at least for 0.5 and 1.0 mg/ml at 40 °C. Our hypothesis of random association between PNIPAM and PnBA units at 25 °C supports the capability of the micelles to increase their aggregation number as hydrophobicity of PNIPAM is abruptly increased (phase transition). In addition if a separate PnBA (core) – PNIPAM (shell) formulation was the case then a shrinkage of the shell thickness would be expected. For the rest of the cases (2.0 and 4.0 mg/ml at 40 °C and all concentrations at 50 °C) there is an apparent drop in the micellar aggregation numbers although the radii do not change significantly. Since in the calculation of aggregation number the nominal solution mass concentration is taken as the mass concentration of micelles we conclude that in the certain cases the population of micelles is reduced and their chains are incorporated in the large aggregates in a different conformation. This trend is followed by the micellar forward scattering I_0 which is proportional to concentration up to 1.0 mg/ml at 40 °C and not for the rest of the samples (table 1).

At room temperature volume fraction profile exponent ($a\sim1.7$) is between $a = 4/3$ which is characteristic of neutral spherical brushes and $a = 2$ for osmotic polyelectrolyte brushes[27]. Apparently the charged single terminating group cannot provide any significant radial stretching as in polyelectrolyte brushes where $a\sim2$. The deviation of the exponent from the neutral one is due to the hydrophobic interactions (strong PnBA-PnBA, weak PNIPAM-PNIPAM) present within the shell that can create tendency for relatively higher volume fractions towards the core. The increase of the exponent a of the volume fraction profile upon the phase transition of PNIPAM shows the magnification of the previous efect by the greatly enhanced PNIPAM-PNIPAM hydrophobic interactions.

The values of G_{agg} at low temperature are proportional to concentration as the shape of the SANS curves is concentration independent. Although the Guinier regime of the large aggregates is not inside the SANS q-range and therefore R_g and G_{agg} cannot be independently defined, we can still compare the scattering strengths G_{agg} between samples when R_g and d_{agg} have similar values for different samples. At 40 °C the drop of $d_{agg}$to 1.81 (2mg/ml) and then back to ~4 (4mg/ml) signifies the gradual enhancement of fractal aggregates as concentration increases. At 50 °C (except from 4mg/ml) d_{agg} is near 3 which is relevant to rough surface or dense mass fractal[33]. This is different than in 25 and 40 °C where the fractal exponent is the one of well defined interfaces. Probably the secondary aggregation at very high temperature results in random packing of the initially formed aggregates. Intrarmicellar scattering is virtually unaffected at all situations with $d_{int}\sim2$ although there is some tendency of increase at the highest temperature. This exponent arises from the mass fractal spatial arrangements of hydrophobic domains within the shells that are virtually not affected by temperature[16].

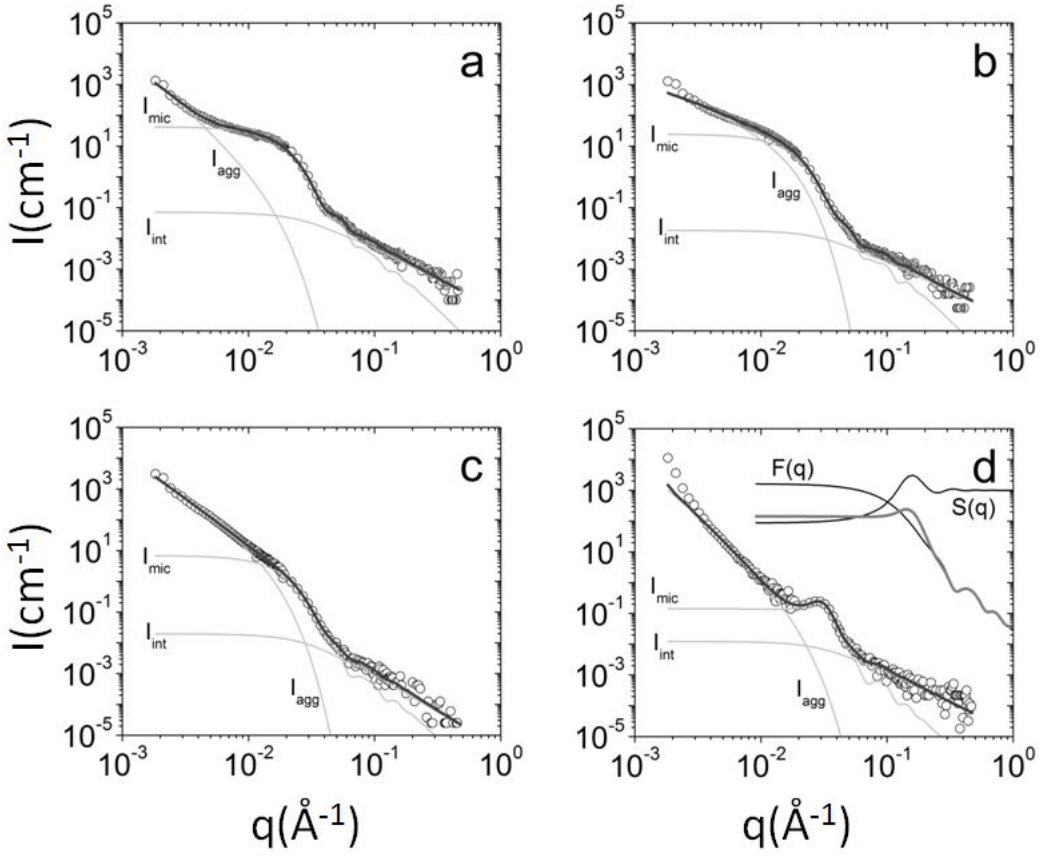

Figure 6: Representative fits of SANS data from PnBA-b-PNIPAM-COOH for (a) 4.0 mg/ml 25 °C, (b) 2.0 mg/ml 40 °C, (c) 1.0 mg/ml 50 °C and (d) 4.0 mg/ml 50 °C. The separate contributions of equation 4 are shown. In (d) the micellar scattering factor is also analyzed in the separate form F(q) and structure S(q) factors.

Equation 4 fits the data at all concentrations for all temperatures (figure 6). For 4.0 mg/ml the Percus–Yevick approximation for hard-sphere interactions is employed[16, 34] to incorporate a structure factor $S(q)$ into the micellar scattering term. Incorporation of a structure factor was necessary beacause the SANS data from 4.0 mg/ml are qualitatively different than at the rest of the concentrations. The correlation peak cannot be fitted by the micellar or aggregate form factor (this treatment will be also used for all lysozyme containing samples at high temperature). Interactions in this system maybe complicated by the "softness" of the core-shell micelles, the

"stickyness" of the hydrophobic segments and the presence of charges. Nevertheless the hard sphere approximation adequately fits the data without the need of introducing more complicated models and keeping the fitting parameters at the minimum number (only two). Then the results can be phenomenologically interpreted in comparison to the rest of the SANS obtained parameters. In equation 7 $I_{mic}(q)$ is replaced by $I_{mic}(q) \cdot S(q; \varphi_{hs}, D_{hs})$ where φ_{hs} is the volume fraction and D_{hs} the diameter of interacting hard spheres. The resulting $D_{hs} \approx 19nm$ is smaller than micellar diameter $2R_m \approx 36nm$ but not much higher than the core diameter $2R_c \approx 13nm$,which means that the micelles are highly interpenetrating as we have observed for flower-like PS-b-PNIPAM-b-PS micelles[16] and interact with their apparently hard core. Conclusively PNIPAM (above LCST) creates dense domains within the core that result to well defined interactions not existing below the LCST. Effective volume fraction ($\varphi = 25\%$) is two orders of magnitude higher than the solution volume fraction. Obviously the correlation peak comes from micelles that while being confined within the large aggregates have a degree of mobility relatively to each other.

Comparison of SANS with LS shows interesting complementarity. The separate small length-scale population that exists below 40 °C (figure 2 and 3) increases from 15 to 23 nm. Hence this population is identified by SANS as individual core-shell micelles that have similar radius (table 1) with a similar trend to increase with temperature both in size and aggregation number. Above the transition temperature the large-size population dominates DLS and it is greatly increased as seen by SLS intensity. Nevertheless SANS still distinguishes the presence of micelles within the aggregates in an hierarchical manner. In SANS forward scattering (which is defined by the aggregates) also increases. The two methods are performed at different concentrations and because of the documented sensitivity of the large-scale aggregation on

concentration in the SANS data of this work and elsewhere[16] is not expected[22] to be identical. Except from the hydrophobic interactions between PNIPAM-PNIPAM, PnBA-PnBA and PNIPAM-PnBA blocks of diffferent micelles, hydrogen bonding[17] between the COOH end-groups may also contribute to the intermicellar aggregation.

Complexation of PnBA-b-PNIPAM-COOH with lysozyme

The hydrodynamic radius of aggregates decreases as lysozyme is added to the solution (at room temperature), while the micellar radius appears rather unaffected (figure 7b). The SLS intensity (figure 7a) is overall slightly decreasing which is a sign of possible disassociation of the large aggregates to smaller ones that is followed naturally by the drop of their size. Above 0.1 mg/ml lysozyme there is no detectable presence of free micelles in solution pointing to their incorporation into large aggregates with the bridging between intermicellar COO^- units by lysozyme globules being possibly the most effective mechanism below the LCST. It has to be noted that the hydrodynamic radius of lysozyme[4] was confirmed by our DLS measurements to be not more than 2 nm. Hence it is three times smaller than the smallest characteristic length-scale in this system (core radius). The effects of lysozyme on micellar and aggregate overall size and morphology comes from the interactions with the macromolecular segments.

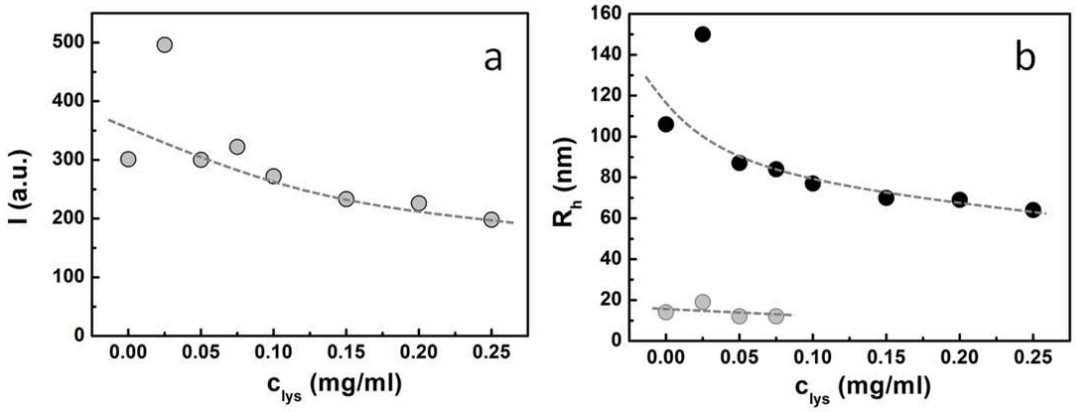

Figure 7: (a) SLS intensity and (b) hydrodynamic radii (DLS) of micelles (●) and aggregates (●) as a function of added lysozyme concentration in PnBA-b-PNIPAM-COOH solutions ($c = 0.01\ mg/ml$). Dashed lines are guides to the eye.

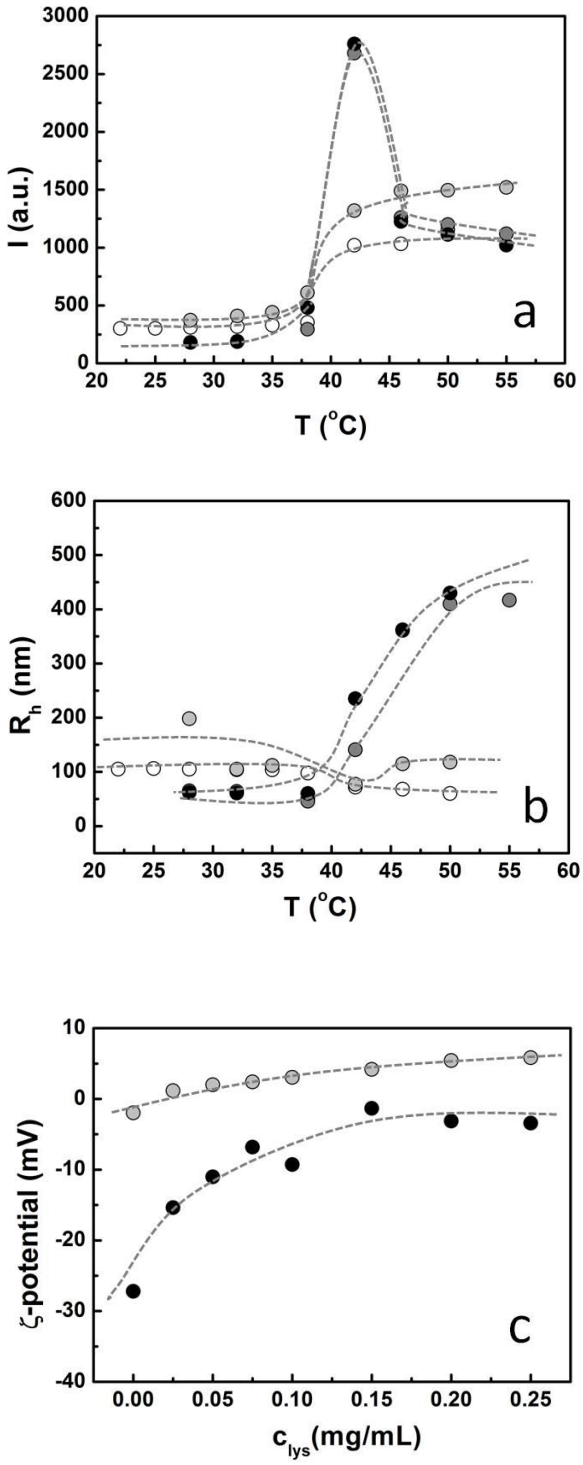

Figure 8: (a) SLS intensity and (b) hydrodynamic radii (DLS) of aggregates for 0 (○), 0.025 (●), 0.1 (●) and 0.25 (●) mg/ml lysozyme added to PnBA-b-PNIPAM-COOH solutions ($c = 0.01\, mg/ml$). (c) ζ-Potential (electrophoretic LS) of PnBA-b-PNIPAM-COOH/LYZ complexes at 25 (●) and 43 (●) °C. Dashed lines are guides to the eye.

The SLS intensity of complexes increases as the temperature rises above the LCST in a manner roughly similar to the one of non-complexed aggregates (figure 8a). The two solutions with highest amount of lysozyme show a strong maximum in intensity at about 40-45°C. These two cases are the ones that strongly deviate from the temperature induced R_h variation of the non-complexed aggregates (figure 8b). They create roughly four times larger aggregates than the rest of the complexes. This difference in size, without significant difference in molecular weight, could highlight a more loose conformation for the complexes with higher protein content at high temperatures. Perhaps the initially formed high molecular weight aggregates (intensity maximum at intermediate temperatures) break to lighter and more loose aggregates where the effect of PNIPAM shrinking is somehow neutralized by the presence of lysozyme globules. This points to the scenario that complexation of lysozyme, due to hydrophobic interaction with PNIPAM segments, may hinder thermoresponsive conformational changes[17]. At room temperature the non-complexed aggregates have negative ζ-potential but it is inverted even at the lowest added amount of lysozyme (figure 8c). So lysozyme globules attach to the aggregates even when the COO^- units charge is neutralized. When the complexed and non-complexed aggregates are brought to 43 °C their surface charge increases i.e. COO^- units are presumably pushed away from the highly hydrophobic interior and they dominate the surface potential

even at the highest amount of lysozyme. Still the presence of attached lysozyme is highlighted by a gradual increase of the ζ-potential.

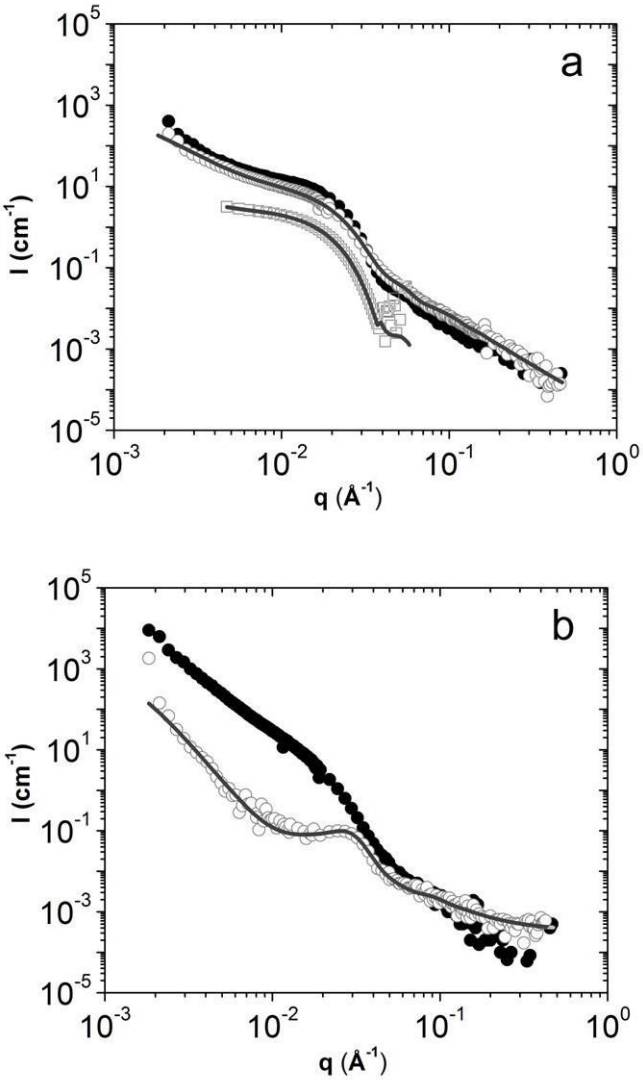

Figure 9: SANS data from PnBA-b-PNIPAM-COOH (2.0 mg/ml)/LYZ (0.1 mg/ml) complexes at 25 (a) and 50 (b) °C. Both cases of added (○) and no added (●) lysozyme are presented. The lysozyme contrast matched PnBA-b-PNIPAM-COOH (2.0 mg/ml)/LYZ (0.1 mg/ml) complexes (□) are shown in (a). Lines are fits with equation 4.

As we exploited the potential of solvent contrast variation of the system we tested lysozyme (D_2O/H_2O at 42/58 v/v) and polymer (D_2O/H_2O at 20/80 v/v) contrast matching solvents for the complexed samples. Because of the high H_2O content the

incoherent q-independent background was significant and dominated the high-q range. On the other hand the low-q range (long camera lengths) was too weak to be measured because of the dramatically reduced solvent/solute neutron scattering length density contrast. By optimizing camera length and neutron wavelength we managed to obtain data with adequate statistics at 12m camera length and λ=0.506nm only for the case of room temperature and lysozyme contrast matching solvent where the SANS intensity was strong enough (figure 9a). The q-range obtained for the contrast matched solution is dominated by the micellar scattering term. The data were fitted by setting the water contrast equal to the one of the mixed solvent and using the same fitting procedures as with pure D_2O (see table 2 for fitting parameters).

At room temperature the SANS profile of the complexed sample is clearly different in shape than the non-complexed one (figure 9a). Addition of lysozyme does not influence the core or micellar lengths (table 2). The alteration in SANS profile shape (figure 9a) is captured by an increase in exponent a and the aggregation numbers. A steeper volume fraction profile is a hint of accumulation of lysozyme globules near the core of the micelles instead of a uniform distribution of globules that follows the initial shell morphology. The SANS profiles do not show any sign of lysozyme form factor or globule-globule correlations. This is possibly due to the small size of lysozyme and the dominance of micellar blob scattering at high q. For that reason its presence within a micelle is quantified by the azimuthally averaged volume fraction profile. The apparent drop of N_{in} and N_{out} is not resolved to absolute numbers of lysozyme and macromolecular chains. The uncertainty of the actual micellar concentration (as part of a total micellar and aggregate concentration) is the main reason for this. Additionally it is not certain that the micellar aggregation numbers remain the same upon complexation with lysozyme. For the samples where lysozyme

is “invisible” from neutrons (lysozyme contrast matched) the scattering profiles are steeper than the non matched samples and resemble the ones with no added lysozyme (figure 9a). The fits result to volume fraction exponents ($a \approx 1.7$) similar to the ones in the absence of lysozyme i.e. the steepness of the overall volume fraction profile ($a \approx 2$) is indeed caused by the incorporation of lysozyme globules towards the core. The fractal aggregates forward scattering drops as lysozyme is added to the solution in agreement with the LS results where there are signs of possible dissociation of the large aggregates although not down to values 60-70nm observed by LS.

Table 2: SANS extracted parameters for PnBA-b-PNIPAM-COOH (2.0 mg/ml) mixtures with lysozyme at the studied concentrations and temperatures.

LYZ. $(\frac{mg}{ml})$***/*** ***Param.***	**25 °C**					**50 °C**		
	0.0	0.1	0.2	0.1*	0.2*	0.0	0.1	0.2
$R_c(nm)$	6.0	6.0	6.0	6.1	6.0	6.4	6.4	6.3
$R_m(nm)$	16.6	16.4	16.5	16.6	16.1	18.0	14.0	14.2
$t_s(nm)$	10.6	10.4	10.5	10.5	10.1	11.7	7.6	7.9
N_{in}	49	31	28	30	26	31	2	1
N_{out}	241	118	104	184	147	134	3	2
N_{tot}	290	148	132	214	173	165	5	3
a	1.73	1.99	1.97	1.71	1.71	2.30	2.29	2.12
$I_0(cm^{-1})$	22.5	11.5	8.9	2.99	2.35	12.8	0.40	0.24
$G_{agg}(cm^{-1})$	4710	1300	1310			264000	1660	1470
d_{agg}	3.93	2.56	2.51			2.95	4.69	4.85
$R_g(nm)$	161	172	168			359	167	169

d_{int}	2.03	2.43	2.00			2.60	2.02	1.86
φ_{hs}							0.22	0.23
D_{hs}							19.0	19.7

*LYZ contrast matched samples.

The effect of lysozyme complexation is very intense at increasing temperature above the LCST of the system (50 °C). While the non-complexed sample at this concentration did not show the transition to the hard-sphere interacting micelles trapped within large aggregates, the presence of protein forces the system towards this behavior. This transition needed high polymer content to occur in the absence of lysozyme. The effect of lysozyme might be connected to the neutralization of COO^- units that otherwise would stabilize the system at least up to 2.0 mg/ml PnBA-b-PNIPAM-COOH. Effectively lysozyme acts here as a tuning factor for the morphological transitions upon temperature changes. The characteristic interaction diameter is somewhat higher than the case of no added protein. This would show that incorporation of lysozyme globules expands the hard core. The additional hydrophobic content introduced to the core by lysozyme forces the system to phase separate in clusters of interacting spheres at lower concentrations. Non-specific interactions between proteins and PNIPAM have been proved by protein adsorption on PNIPAM thermoresponsive surfaces[35]. In particular lysozyme refolding from a denatured state has been shown to be assisted by PNIPAM spherical brushes[36]. Finally it has to be noted that lysozyme is stable up to 70º C in similar solution conditions so we do not expect any alteration in its structure caused by temperature[37].

Conclusions

The hierarchical morphology of PnBA-b- PNIPAM-COOH was characterized in detail by scattering techniques. Combination of DLS with SANS confirms the existence of two separate populations in aqueous solutions. While DLS shows that single micelles and aggregates are present SANS distinguishes the separate contributions. The calculations on the scattering length density profiles reveal that PMIPAM and PnBA coexist in both the dense core and the hydrated micellar coronas. This is explained by the inherent hydrophobic content of PNIPAM at room temperature. Above the LCST micellar aggregation is enhanced as seen in the increase in core and shell size and volume fraction profile exponent. Aggregation of micelles is increased as temperature increases and this response is sensitive to the solution concentration. At the highest concentration studied micelles show interacting hard-sphere correlations defined by core-core interactions. Overall the temperature response of morphology in this complex system appears to depend on the hierarchy level. Micellar aggregation (low q) is greatly sensitive to both temperature and concentration, micellar morphology (intermediate q) changes as temperature rises and intra-micellar blob scattering (high q) is unaffected by neither temperature or concentration. ζ-potential measurements revealed that the hydrophilic charged end groups are exposed to the outer aggregate surface. Lysozyme globules appeared to bind near the micellar cores a finding that was supported by SANS measurements in contrast matched lysozyme. Incorporation of protein globules reinforced the hydrophobic effects and led to hard-sphere correlations within the aggregates instead of self-similar fractal morphology above the LCST. This structure needed the highest polymer concentration to form in the absence of protein. The presented study demonstrates the use of small angle scattering in macromolecular self-assembled nanostructures that combine protein interactions and temperature response.

Acknowledgements

The authors acknowledge financial support by the NANOMACRO 1129 project which is implemented in the framework of the Operational Program “Education and Life-long Learning” of the National Strategic Reference Program-NSRF (Action

"ARISTEIA I") and it is co-funded by the European Union (European Social Fund-ESF).

This research project has been supported by the European Commission under the 7th Framework Programme through the 'Research Infrastructure' action of the 'Capacities' Programme, NMI3-II Grant number 283883.

References

1. A. B. Kayitmazer, D. Seeman, B. B. Minsky, P. L. Dubin and Y. Xu, *Soft Matter*, 2013, **9**, 2553-2583.
2. E. Seyrek, P. L. Dubin, C. Tribet and E. A. Gamble, *Biomacromolecules*, 2003, **4**, 273-282.
3. S. Rosenfeldt, A. Wittemann, M. Ballauff, E. Breininger, J. Bolze and N. Dingenouts, *Phys. Rev. E*, 2004, **70**, 061403.
4. F. Cousin, J. Gummel, D. Ung and F. Boué, *Langmuir*, 2005, **21**, 9675-9688.
5. K. Henzler, B. Haupt, K. Lauterbach, A. Wittemann, O. Borisov and M. Ballauff, *J. Am. Chem. Soc.*, 2010, **132**, 3159-3163.
6. R. A. Silva, M. D. Urzúa, D. F. S. Petri and P. L. Dubin, *Langmuir*, 2010, **26**, 14032-14038.
7. W. Zhang, L. Shi, K. Wu and Y. An, *Macromolecules*, 2005, **38**, 5743-5747.
8. C. L. McCormick, B. S. Sumerlin, B. S. Lokitz and J. E. Stempka, *Soft Matter*, 2008, **4**, 1760-1773.
9. C. Wu and X. Wang, *Phys. Rev. Lett.*, 1998, **80**, 4092-4094.
10. D. Schmaljohann, *Adv. Drug Deliv. Rev.*, 2006, **58**, 1655-1670.
11. M. A. C. Stuart, W. T. S. Huck, J. Genzer, M. Muller, C. Ober, M. Stamm, G. B. Sukhorukov, I. Szleifer, V. V. Tsukruk, M. Urban, F. Winnik, S. Zauscher, I. Luzinov and S. Minko, *Nat. Mater.*, 2010, **9**, 101-113.
12. M. A. Ward and T. K. Georgiou, *Polymers*, 2011, **3**, 1215.
13. A. Papagiannopoulos, J. Zhao, G. Zhang, S. Pispas and A. Radulescu, *Polymer*, 2013, **54**, 6373-6380.

14. J. Adelsberger, E. Metwalli, A. Diethert, I. Grillo, A. M. Bivigou-Koumba, A. Laschewsky, P. Müller-Buschbaum and C. M. Papadakis, *Macromol. Rapid Commun.*, 2012, **33**, 254-259.
15. J. Adelsberger, I. Grillo, A. Kulkarni, M. Sharp, A. M. Bivigou-Koumba, A. Laschewsky, P. Muller-Buschbaum and C. M. Papadakis, *Soft Matter*, 2013, **9**, 1685-1699.
16. A. Papagiannopoulos, J. Zhao, G. Zhang, S. Pispas and A. Radulescu, *Eur. Polym. J.*, 2014, **56**, 59-68.
17. A. Papagiannopoulos, A. Meristoudi, K. Hong and S. Pispas, *Polymer*, 2016, **83**, 111-115.
18. J. Škvarla, J. Zedník, M. Šlouf, S. Pispas and M. Štěpánek, *Eur. Polym. J.*, 2014, **61**, 124-132.
19. U. Keiderling, *Appl. Phys. A*, **74**, s1455-s1457.
20. J. G. Barker and J. S. Pedersen, *J. Appl. Crystallogr.*, 1995, **28**, 105-114.
21. D. Vanderbilt and S. G. Louie, *J. Comput. Phys.*, 1984, **56**, 259-271.
22. A. Papagiannopoulos, M. Karayianni, G. Mountrichas, S. Pispas and A. Radulescu, *Polymer*, 2015, **63**, 134-143.
23. B. J. Berne and R. Pecora, *Dynamic Light Scattering, With Applications to Chemistry, Biology, and Physics*, Dover, Toronto, 2000.
24. J. Zhao, G. Zhang and S. Pispas, *J. Polym. Sci. A Polym. Chem.*, 2009, **47**, 4099-4110.
25. J. Yan, W. Ji, E. Chen, Z. Li and D. Liang, *Macromolecules*, 2008, **41**, 4908-4913.
26. A. Müller and W. Burchard, *Colloid Polym. Sci.*, 1995, **273**, 866-875.
27. S. Förster, N. Hermsdorf, C. Böttcher and P. Lindner, *Macromolecules*, 2002, **35**, 4096-4105.
28. B. Hammouda, *J. Appl. Crystallogr.*, 2010, **43**, 1474-1478.
29. J. S. Higgins and H. C. Benoit, *Polymers and Neutron Scattering*, OUP, 1994.
30. M. P. Allen and D. J. Tildesley, *Computer Simulation of Liquids*, Oxford Science Publications, Clarendon Press, Oxford, 2001.
31. A. Papagiannopoulos, M. Karayianni, G. Mountrichas, S. Pispas and A. Radulescu, *J. Phys. Chem. A*, 2010, **114**, 7482-7488.
32. G. Bokias, D. Hourdet, I. Iliopoulos, G. Staikos and R. Audebert, *Macromolecules*, 1997, **30**, 8293-8297.

33. P. Schmidt, *J. Appl. Crystallogr.*, 1991, **24**, 414-435.
34. J. S. Pedersen, *Adv. Colloid Interface Sci.*, 1997, **70**, 171-210.
35. X. Cheng, H. E. Canavan, D. J. Graham, D. G. Castner and B. D. Ratner, *Biointerphases*, 2006, **1**, 61-72.
36. X. Ge, Y.-X. Guan, J. Chen, Z. Yao, K. Cao and S.-J. Yao, *J. Appl. Polym. Sci.*, 2009, **114**, 1270-1277.
37. A. Blumlein and J. J. McManus, *BBA PROTEINS PROTEOM*, 2013, **1834 (10),** 2064-2070.

for Table of Contents use only

Effect of Lysozyme Complexation on the Thermoresponsive Behavior of Micellar Aggregates from end-functionalized PnBA-b-PNIPAM-COOH Block Copolymers

Aristeidis Papagiannopoulos[1,*], Anastasia Meristoudi[1], Stergios Pispas[1,*] and Uwe Keiderling[2]

[1]Theoretical and Physical Chemistry Institute, National Hellenic Research Foundation, 11635 Athens, Greece

[2]Helmholtz Zentrum Berlin, D-14109 Berlin, Germany

* pispas@eie.gr

* apapagiannopoulos@eie.gr

The thermoresponsive transition of PnBA-b-PNIPAM-COOH micellar aggregates to clusters of interacting micelles is enhanced by the presence of lysozyme.